J Mol Model (2013) 19:5097–5112
DOI 10.1007/s00894-013-1997-3

ORIGINAL PAPER

Binding selectivity studies of PKBα using molecular dynamics simulation and free energy calculations

Shi-Feng Chen · Yang Cao · Jiong-Jiong Chen · Jian-Zhong Chen

Received: 13 May 2013 / Accepted: 4 September 2013 / Published online: 2 October 2013

Abstract Designing selective protein kinase B (PKB/Akt) inhibitor is an area of intense research to develop potential anticancer drugs. In the present study, the molecular basis governing PKB-selective inhibition has been investigated using molecular dynamics simulation. The binding free energies calculated by MM/PBSA gave a good correlation with the experimental biological activity and a good explanation of the activity difference of the studied inhibitors. The decomposition of free energies by MM/GBSA indicates that the ethyl group on pyrrolo[2,3-*d*]pyrimidine ring of inhibitor Lig1 (N-{[(3*S*)-3-amino-1-(5-ethyl-7*H*-pyrrolo[2,3-*d*]pyrimidin-4-yl)pyrrolidin-3-yl]-methyl}-2,4-difluoro-benzamide) is an important contributor to its PKBα selectivity due to its hydrophobic interaction with the side chain of Thr291 in PKBα. The substituted groups on the pyrrolidine ring of Lig1 also show a strong tendency to mediate protein-ligand interactions through the hydrogen bonds formed between the amino or amide groups of Lig1 and the carboxyl O atoms of Glu234, Glu278, and Asp292 of PKBα. It was reported that there are only three key amino acid differences between PKBα (Thr211, Ala230, Met281) and PKA (Val104, Val123, Leu173) within the clefts of ATP-binding sites. These differences propel a drastic conformational change in PKA, weakening its binding interactions with inhibitor. The impact was also confirmed by MD simulated interaction modes of inhibitor binding to PKBα mutants with the *in silico* mutations of the three key amino acids, respectively. We expect that the results obtained here could be useful for future rational design of specific ATP-competitive inhibitors of PKBα.

S.-F. Chen · Y. Cao · J.-J. Chen · J.-Z. Chen (✉)
Institute of Materia Medica, College of Pharmaceutical Sciences, Zhejiang University, 866 Yuhangtang Rd, Hangzhou, Zhejiang 310058, China
e-mail: chjz@zju.edu.cn

Keywords Binding free energy · Inhibitor · Molecular dynamics simulation · Protein kinase A/PKA · Protein kinase B/PKB · Selectivity

Abbreviations

PKB/Akt	Protein kinase B
MD	Molecular dynamics
PKA	Protein kinase A

Introduction

Protein kinase B (PKB, also known as Akt) [1, 2] is a serine/threonine protein kinase. It is a downstream target for phosphatidylinositol 3-kinase (PI3K) to play an important role in PI3K-Akt-mTOR pathway. Activated PKB can control cell signaling processes by phosphorylating endogenous substrates which are involved in glucose metabolism, cell growth, survival, apoptosis, cell migration and transcription. PKB activity is frequently elevated in tumor due to several reasons, including the amplification and function mutations of upstream receptor tyrosine kinases and PI3K, as well as functional loss of PTEN, a negative regulator of PKB. Aberrant PKB signaling has been observed in a number of human cancers, including breast, prostate, ovarian carcinoma, and melanoma. PKB belongs to AGC protein kinase superfamily [3]. It was identified as a homology protein of protein kinase A (PKA), sharing 65 % homology with PKA [4]. There are three subtypes of human PKBs, including PKBα/Akt-1, PKBβ/Akt-2, and PKBγ/Akt-3, which share a more than 80 % homology with each other [3, 5]. The major isoform PKBα is ubiquitously expressed at high levels [6] and has become a target for anti-tumor therapy [7]. There are a few PKBα inhibitors studied in clinical trials for the treatment of tumor, such as ATP-competitive inhibitors GSK690693 (4-(2-(4-amino-1,2,5-oxadiazol-3-yl)-1-ethyl-

7-((*S*)-piperidin-3-ylmethoxy)-1*H*-imidazo[4,5-*c*]pyridin-4-yl)-2-methyl-but-3-yn-2-ol)[8] and GDC-0068 (2-(4-chlorobenzyl)-1-(4-((5*R*,7*R*)-7-hydroxy-5-methyl-6,7-dihydro-5*H*-cyclo-penta[*d*]-pyrimidin-4-yl)piperazin-1-yl)-3-(isopropyl-amino)-propan-1-one)[9] (Fig. 1). GDC-0068 is currently under evaluation in clinical trials against cancer with quite good selectivity (PKBα: IC_{50}=5 nM, PKA: IC_{50}=3100 nM, PKA selectivity ratio=620). GSK690693 is also a highly potent inhibitor of Akt kinases with IC_{50} value of 2 nM for PKBα, but it is less selective for other members of the AGC kinase family, like PKA (IC_{50}=24 nM) and PrkX (IC_{50}=5 nM). Therefore, the clinical phase I trial of GSK690693 was terminated in 2010. These results indicated that PKB inhibitor should be developed with higher specificity for PKBα over PKA.

With empirical or knowledge-based scoring functions, structure-based molecular modeling and graphic analyses have been undertaken to elucidate characteristically the selective mechanism of PKBα inhibition [7, 10–12]. For example, Freeman-Cook *et al*. proposed an effective strategy to maintain PKBα selectivity of the inhibitor by increasing the steric demands of its substituents which are better tolerated in the binding pocket of PKBα than PKA [7]. Xu *et al*. concluded that the inhibitor's selectivity to PKB over PKA can be modulated by increasing the size of its substituent, which has hydrophobic interaction with PKBα's hinge region near the gatekeeper residue Met227 [10]. Kallan *et al*. hypothesized that the different hinge interactions, which are critical for the activity, may be responsible for PKBα selective inhibition [11].

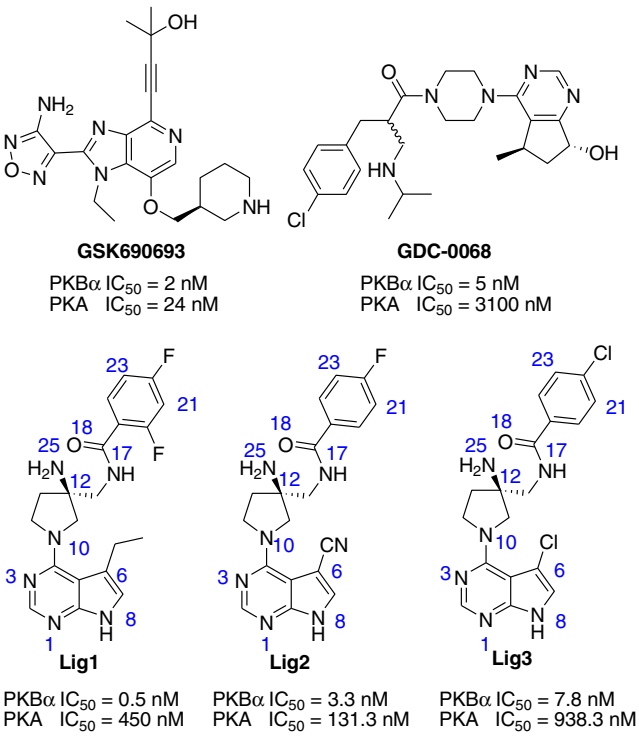

Fig. 1 The structures and IC_{50}s of PKB inhibitors GSK690693[8], GDC-0068[9], Lig1, Lig2, and Lig3[7]

By coupling the results from the X-ray structures of PKBα and PKA and biological evaluation, Bencsik *et al*. put forth their proposal on the differences of three key amino acid within the ATP-binding sites between PKBα (Thr211, Ala230, Met281) and PKA (Val104, Val123, Leu173), since there is a narrower cavity in PKA than in PKB. Hydrophilic substituents in the vicinity of Thr211 and the bound water would be expected to improve selectivity over PKA [12].

As an important technology and tool to study interaction mechanism for ligand-receptor complex, molecular dynamic (MD) simulations and free energy calculations have been widely applied for the studies of the selectivity of different kinase inhibitors in recent years [13–16]. Free energy calculations have been frequently performed to evaluate the binding affinities of ligands and further predict their bioactivities and influences on the stabilities of biomolecular structures. By integrating molecular mechanics energy and continuum solvation models, molecular mechanics/Poisson Boltzmann surface area (MM/PBSA)[17] and molecular mechanics/generalized Born surface area (MM/GBSA)[18] were developed for the free-energy calculations and molecular docking studies of ligand binding to its receptor. MM/PBSA and MM/GBSA are indeed more specific than most empirical or knowledge-based scoring functions. In addition, the binding statues variation due to the flexibility of the pocket could be clearly evaluated with the implementation of MM/PBSA and MM/GBSA methods based on the MD simulation. Moreover, both MM/PBSA and MM/GBSA allow for rigorous free-energy decomposition into contributions originating from different groups of atoms or types of interactions, which could predict both key residues around the binding pocket and pharmaceutical features within ligand playing critical roles in ligand's bioactivity. As the MD simulation and free energy calculations can predict the ligand's affinity rapidly, intuitively and effectively, the popular MM/PBSA and MM/GBSA methods have been successfully applied to the study of a variety of protein systems [13, 16, 19, 20]. However, no one has employed MD simulation and free energy calculations to analyze the mechanism of PKBα selective inhibition.

In the present study, we performed MD simulations, free energy calculations on the inhibitors with different selectivity binding to PKA or PKB to study the interaction mode and selective mechanism. As reported, N-{[(3*S*)-3-amino-1-(5-ethyl-7*H*-pyrrolo[2,3-*d*]pyrimidin-4-yl)pyrroli-din-3-yl]methyl}-2,4-difluorobenzamide (compound Lig1 in Fig. 1) displays 900-fold greater selectivity for PKBα than PKA, while inhibitors Lig2 and Lig3 have moderate selectivity [7]. These three ligands taken up in this study contain the steric substituents, proposed to be essential requirements for PKBα selectivity. By comparing the structures of inhibitors Lig1, Lig2, and Lig3, [7] it was observed that there is a tremendous selectivity toward PKBα after the introduction of a C-6 substituted ethyl group on pyrrolo[2,3-*d*]pyrimidine ring and a C-12 substituted *N*-methylbenzamide group on pyrrolidine ring. However, to the

best of our knowledge, a detailed insight into the role of the C-6 substituted ethyl group on pyrrolo[2,3-*d*]pyrimidine ring and the C-12 substituted *N*-methylbenzamide group on pyrrolidine ring in PKBα selectivity remains to be investigated. It is essential to inspect how the topological changes are induced by the three key amino acids in the binding pocket of PKBα (Thr211, Ala230, and Met281) compared to PKA (Val104, Val123, Leu173). The effect of the different residues on the ligand's binding with PKA should also be observed. Thus, to improve our understanding of selective mechanism for PKBα inhibition and to assist future structure-based drug design of selective PKB's inhibitor, we employed computational methods to investigate the role of individual residues in ligand binding. A molecular dynamics study of wide type PKBα versus three mutants (*in silico* mutations at positions of Thr211, Ala230, and Met281, respectively, in PKBα) in the presence of compound Lig1 was undertaken primarily to address the above objectives. In addition, a combined computational approach of MD simulation, MM/PBSA free energy calculations, and MM/GBSA free energy decomposition analysis was performed to another two PKB's inhibitors Lig2 and Lig3 (Fig. 1) binding with PKBα and PKA, respectively. It is expected that the obtained results can help to understand the binding process and provide some insights into the further rational design of novel, potent, and selective PKBα inhibitor.

Methods

Initial structure preparation

The co-crystal structure of PKBα with its inhibitor Lig1 (PDB entry: 3MVH[7]) was obtained from the RCSB Protein Data Bank (PDB). The structure of 3MVH was taken as the starting point for the following calculations. Inhibitors Lig2 and Lig3 were prepared by modifying structure of Lig1 extracted from the co-crystal structure of complex PKB-Lig1 using Sketch module in SYBYL-X 1.3 [21]. The *in silico* generated conformations of Lig2 and Lig3 were respectively inserted into the binding pocket of 3MVH to replace Lig1 for the initial structures of the complexes PKB- Lig2 and PKB-Lig3.

Due to the high homology structures among the different protein kinases, the initial structures of our studied inhibitors Lig1, Lig2, and Lig3, respectively, binding to PKA were generated for MD simulations as follows. At first, the crystallographic structure of PKA (PDB entry: 3OW3[12]) was downloaded from the RCSB Protein Data Bank. The obtained structure of PKA was then superimposed with our previously generated structures of three different PKBα-inhibitor complexes, respectively. Each inhibitor was then extracted from its complex with PKBα and merged into PKA to construct the primary PKA-ligand complex model.

The mutants at position Thr211, Ala230, and Met281, respectively, of PKBα were generated through *in silico* mutations by replacing the corresponding residues of 3MVH with the desired amino acids using the Biopolymer module in SYBYL-X 1.3 [21]. The treated structures of these three PKBα mutants, named as T211V, A230V and M281L, were further submitted to MD simulations for the calculations of their interaction modes with inhibitor Lig1, respectively.

MD simulation

The MD simulations were performed using AMBER11 software package [22]. The missing atoms of PKBα and PKA were added using the leap program in AMBER11. Each complex was immersed in TIP3P[23] water in a truncated octahedron box with a margin distance of 9.0 Å. Cl^- or Na^+ ions were then added to neutralize the systems using LEaP module in AMBER11. The AMBER03 force field [24] was used to establish the potentials of the proteins, while the general AMBER force field (GAFF) [25] was used to establish the potentials of the inhibitors. The atomic charges and atom types were assigned by the Antechamber tool in the Amber software package. Particle mesh Ewald (PME) [26] was employed to calculate the long-range electrostatic interactions. A 10.0 Å cutoff distance was applied for the long-range van der Waals (vdW) energy term. In order to remove any steric conflicts induced during system setup, structural optimizations were first performed on the relaxed water molecules and counter ions in two steps with the harmonic constraint potential of 500 kcal·(mol·Å^2)$^{-1}$ and 10.0 kcal·(mol·Å^2)$^{-1}$, respectively, on all heavy atoms of both protein and ligand. Afterward, the whole system was minimized without any restraint. The above three steps were all executed by 2500 cycles of steepest descent minimization followed by 5000 cycles of conjugate gradient minimization. After system optimization, running MD simulations was started on the systems by gradually heating each system in the NVT ensemble from 0 to 300 K in 100 ps using a Langevin thermostat with a coupling coefficient of 1.0/ps and with a force constant 10 kcal·(mol·Å^2)$^{-1}$ on the complex [27]. Considering about the stability of each complex, additional four steps of MD equilibrations were carried out with decreasing restraint weights of 5 kcal·(mol·Å^2)$^{-1}$, 1 kcal·(mol·Å^2)$^{-1}$, 0.5 kcal·(mol·Å^2)$^{-1}$, and 0.1 kcal·(mol·Å^2)$^{-1}$, respectively, in a time of 100 ps per step at 300 K. Finally, a production run for 16 ns MD simulations were performed under the constant temperature of 300 K in the NPT ensemble with periodic boundary conditions. During MD procedure, the SHAKE algorithm [28] was applied for the constraint of all covalent bonds involving hydrogen atoms. The time step was set to 2 fs. Coordinate trajectories were saved every 1 ps throughout the equilibration runs and every 2 ps throughout the production MD runs; 1000 snapshots of the simulated structures within the last 2 ns stable MD

trajectory at 2 ps intervals were extracted for further binding free energy calculations and decomposition analyses.

Binding free energy calculations

The binding free energies (ΔG_{bind}) of the inhibitors with PKBα, PKBα mutants, PKA were calculated using MM/PB(GB)SA method as implemented in Amber 11[29]. The total binding free energy is estimated as the difference between the complex's free energy (G_{complex}) and the sum of individual protein's free energy (G_{protein}) and inhibitor's free energy (G_{ligand}). It can be calculated using the following equation:

$$\Delta G_{bind} = \Delta H - T\Delta S = G_{complex} - \left(G_{protein} + G_{ligand}\right). \quad (1)$$

Each free energy item in Eq. 1 can be calculated by following equation:

$$\Delta G = \Delta E_{MM} + \Delta G_{sol} - T\Delta S \quad (2)$$

where ΔE_{MM}, ΔG_{sol}, $T\Delta S$ represent the molecular mechanic energy, the solvation free energy, and the conformational entropy upon ligand binding at temperature T, respectively. ΔE_{MM} can be divided into the electrostatic energy (ΔE_{ele}), the van der waals energy (ΔE_{vdW}), and internal energy (ΔE_{int}) (Eq. 3), and the solvation free energy (ΔG_{sol}) can be divided into the polar and the nonpolar parts (Eq. 4):

$$\Delta E_{MM} = \Delta E_{ele} + \Delta E_{vdW} + \Delta E_{int} \quad (3)$$

and,

$$\Delta G_{sol} = \Delta G_{ele,\ sol\ PB(GB)} + \Delta G_{nonpol,\ sol} \quad (4)$$

where $\Delta G_{\text{ele, sol PB(GB)}}$ accounts for the electrostatic contribution to solvation and can be calculated using a Poisson Boltzmann (PB) model [30] or a generalized Born (GB) model [31]; $\Delta G_{\text{nonpol,sol}}$ accounts for the nonpolar contribution to solvation and can be calculated by relating it to the solvent accessible surface area (Å^2) (SASA) [16, 32, 33]. The LCPO (linear combination of pairwise overlaps) method [32] was used to calculate the solvent accessible surface area (SASA) with a solvent-probe radius of 1.4 Å. As illustrated in Eq. (5), $\Delta G_{\text{nonpol,sol}}$ was linearly related to calculated SASA with a surface tension parameter γ of 7.2×10^{-3} kcal·(mol·Å^2)$^{-1}$ and a parameterized b value of 0, which were adopted in many publications [14, 15, 33, 34].

$$\Delta G_{nonpol,sol} = \gamma SASA + \mathrm{b} \quad (5)$$

Finally, the entropy contributions (translation, rotation, and vibration) were obtained by using the Nmode protocol [35]. It can be determined from the following equation:

$$T\Delta S = T(\Delta S_{trans} + \Delta S_{rot} + \Delta S_{vib}). \quad (6)$$

Forty snapshots were extracted from the last 2 ns MD trajectory to calculate the entropic contribution using the normal mode [35]. The minimizations for each snapshot was carried out using the conjugated gradient method with a distance dependent dielectric of $4r_{ij}$ (r_{ij} is the distance between two atoms) until the RMS of the elements of the gradient vector was lower than the threshold of 1.0×10^{-4} kcal·(mol·Å)$^{-1}$.

The experimental binding free energy[36] was calculated from the inhibition constant IC_{50} using the following equation:

$$\Delta G_{exp} \approx -RT \cdot lnIC_{50}, \quad (7)$$

where $R=1.986\times10^{-3}$ kcal·(K·mol)$^{-1}$, T=300 K, and IC_{50} is in molar·mol^{-1}.

Per-residue free energy decomposition analysis

In order to provide insight into the changes that occur in the energetic profile of the interaction over the course of the trajectory, binding free energy were further decomposed to each residue's contribution to ligand using the MM/GBSA program in Amber11 [29]. By compared to total binding free energy calculations, per-residue free energy decomposition could reveal each residue's impact on ligand, which will allow us to analyze more deeply and clearly the binding capability and selectivity of each inhibitor. It can be calculated according to the equation:

$$\Delta G_{inhibior-residue} = \Delta E_{vdW} + \Delta E_{ele} + \Delta G_{ele,sol} + \Delta G_{nonpol,sol} \quad (8)$$

In the above equation, ΔE_{vdW} and ΔE_{ele} are van der Waals and electrostatic interactions, computed by the sander program in Amber11 [29], between each inhibitor and every residue of PKBα or PKA. The polar contribution of solvation ($\Delta G_{\text{ele, sol}}$) was calculated using the generalized Born (GB) model with the parameters developed by Onufriev et al. [37]. The nonpolar contribution of solvation ($\Delta G_{\text{nonpol, sol}}$) was computed based on SASA determined with the ICOSA method [18]. The same snapshots utilized in binding free energy calculations were used.

Results and discussion

Overall structural flexibility and stability of MD results

Sixteen ns MD simulations were run for the nine complexes, including six complexes of inhibitors Lig1, Lig2, and Lig3 with PKBα and PKA, respectively, and another three complexes of Lig1 with three PKBα mutants T211V, A230V and M281L,

respectively. Figure 2a-2i showed the calculated RMSDs for all Cα atoms of proteins, backbone atoms of binding pockets (within 6.5 Å of each ligand), and all heavy atoms of the inhibitors of each saved snapshot during MD simulation in relative to the initial minimized structures of each corresponding system. The RMSD plots indicate that the conformations of the nine systems achieve equilibrium after 4 ns. So it is reasonable to do the binding free energy calculation and free energy decomposition based on the conformations extracted from 4 to 16 ns. The RMSDs of the complexes except M281L-Lig1 fluctuate around ~1.5 Å and ~2.0 Å for protein and ligand, respectively. The M281L-Lig1 has the highest fluctuations among the nine systems. Interestingly, Lig1 seems to have an unstable binding mode with M281L, which is revealed by the highest average RMSD values of 3.33 Å and 1.63 Å for protein and inhibitor, respectively, among the nine systems.

Fig. 2j-2l show the root-mean-square fluctuation (RMSF) versus the residue number for these nine complexes. Each

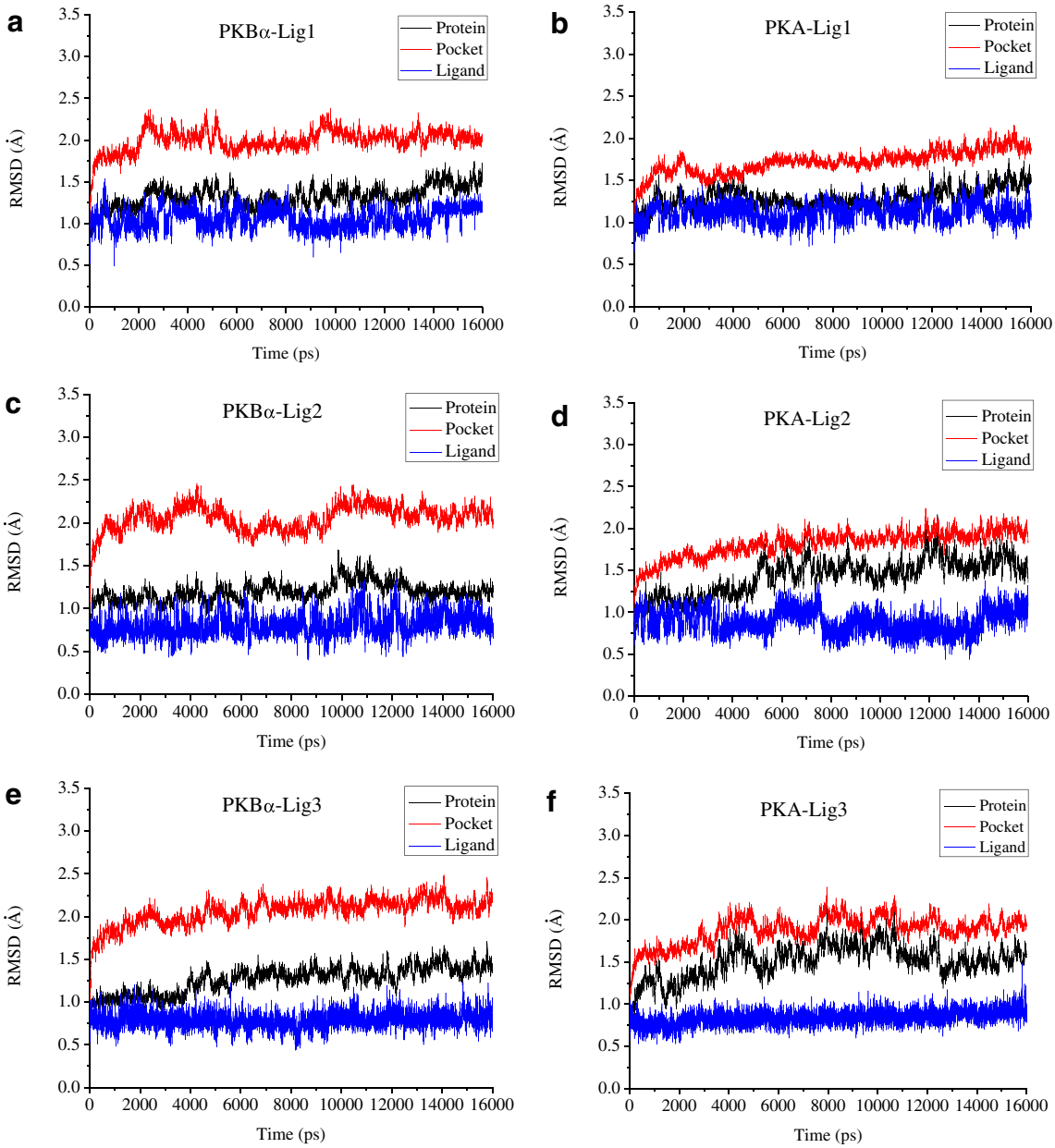

Fig. 2 RMSDs of Cα atoms of the protein, backbone atoms of binding pocket (within 6.5 Å), and the heavy atoms in the ligand for: (**a**) PKBα-Lig1, (**b**) PKA-Lig1, (**c**) PKBα-Lig2, (**d**) PKA-Lig2, (**e**) PKBα-Lig3, (**f**) PKA-Lig3, (**g**) T211V-Lig1, (**h**) A230V-Lig1, (**i**) M281L-Lig1, (**j**) RMSF of each residue of the protein for the complex obtained from the crystal structure and all three PKBα complexes obtained from 16 ns MD simulation, (k) RMSF of each residue of the protein for all three PKA complexes obtained from 16 ns MD simulation, (l) RMSF of each residue of the protein for all three mutants obtained from 16 ns MD simulation

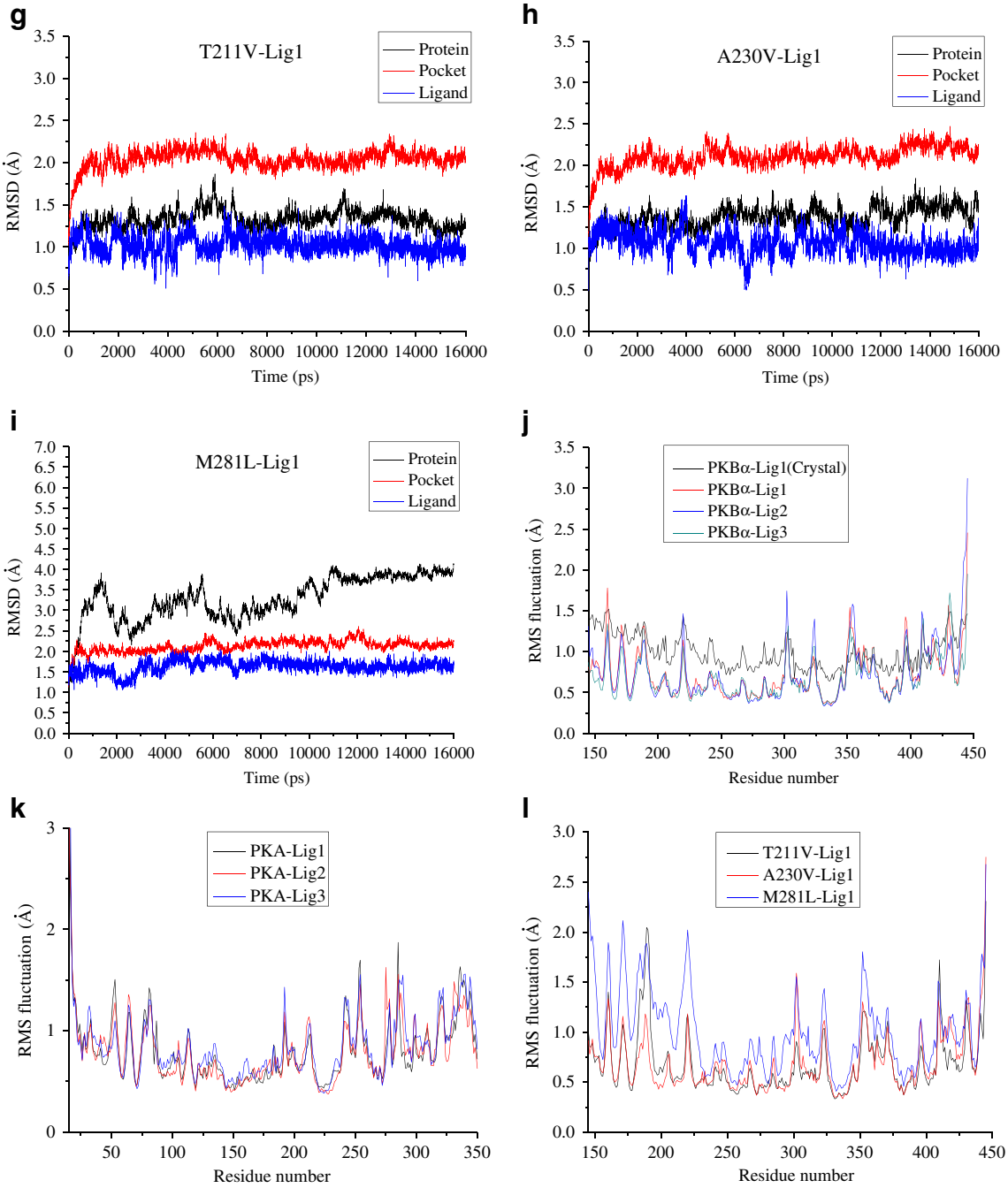

Fig. 2 continued.

RMSF of the PKBα's residues from MD trajectory show similar trend with the results derived from the X-ray crystallographic data, including the residues in the flexible loops with higher fluctuation values. All these data verify the reasonability of the MD results. RMSF profiles of the protein structures of PKBα, PKA and mutants are similar, suggesting that all inhibitors have similar binding modes with PKBα, PKA and mutants. However, it is also observed that the RMSF fluctuation of the active site in M281L-Lig1 is highest among the nine complexes. This result suggests that the binding mode of Lig1 with M281L may be relatively unfavorable as compared to the other eight protein-inhibitor combinations.

Binding free energy calculation

Table 1 summarized the binding free energies of nine systems calculated by the MM/PBSA and MM/GBSA methods in AmberTools 12 [29]. Although the binding free energies

calculated are not equal to the absolute experimental values (ΔG_{exp}) determined by IC_{50}, the changing trends of $\Delta G_{pred\ (GB)}$ values of inhibitors Lig1, Lig2, and Lig3 (−61.49, -51.20, and −42.51 kcal·mol^{-1}, respectively) binding to PKBα are congruent with the changing trends of their experimental IC_{50} values [7] (PKBα: Lig1, IC_{50}=0.5 nM; Lig2, IC_{50}=3.3 nM; Lig3, IC_{50}=7.8 nM). The $\Delta G_{pred\ (GB)}$ values of inhibitors Lig1, Lig2, and Lig3 in PKBα are also lower than those of the inhibitors in PKA, respectively, indicating that these inhibitors bind more tightly with PKBα. On the other hand, the difference of the $\Delta G_{pred\ (GB)}$ values of Lig1 with PKBα and PKA is more significant in comparison to Lig2 and Lig3. This is in accord with the fact that Lig1 is the compound with the best selectivity to PKBα among the three selective inhibitors. Furthermore, $\Delta G_{pred\ (GB)}$ of Lig1 binding to PKBα is more negative than that of each PKBα mutant (T211V, A230V, M281L), indicating that Lig1 binds more tightly with PKBα than three PKBα mutants, and the residues Thr211, Ala230, and Met281 of PKBα could lead to enhanced binding affinity between inhibitor and protein. Therefore, it could be hypothesized that all three residues play critical roles in bioactivity and selectivity of Lig1.

As listed in Table 1, the total binding free energy was decomposed into individual components with MM/PBSA and MM/GBSA, which enabled us to understand the binding process of each complex in detail. Comparisons of the energy components for all nine models reveal that electrostatic interaction is the biggest contributor to ligand's binding to PKBα, three PKBα mutants (T211V, A230V, M281L), and PKA. The noticeable differences of inhibitors Lig1, Lig2 and Lig3 binding to PKBα, PKA, and the PKBα mutants also lie in electrostatic interactions. This finding is not surprising since there are a few charged residues, including Glu228, Ala230, Glu234, Glu278, and Glu292 within 5 Å around each of inhibitors Lig1, Lig2, and Lig3, in the binding pockets of PKBα and each PKBα mutant. Similarly, the three inhibitors binding to PKA are surrounded by its charged residues Glu121, Val123, Glu127, Glu170 and Asp184. However, the favorable Coulomb interactions between protein and inhibitor are counteracted by the unfavorable electrostatics of desolvation, which means that the sum ($\Delta G_{ele}+\Delta G_{ele,\ sol}$) of the electrostatic interaction contributions in vacuum and solvent is unfavorable for the binding of inhibitors in the nine systems [15]. Although E_{vdW} and the nonpolar solvation contribution $\Delta G_{nonpol,\ sol}$ are less important than electrostatic contribution, they also drive the interactions between PKBα, PKA, three PKBα mutants and the inhibitors. The favorable effects of hydrophobic residues with ligand are larger in PKBα than in PKA and three PKBα mutants. Meanwhile, in comparison to Lig2 and Lig3, the differences of the values of ΔG_{ele}, E_{vdw} and $\Delta G_{nonpol,\ sol}$ of Lig1 with PKBα and PKA are more significant. All these data verify that Lig1 has better selectivity toward PKBα than inhibitors Lig2 and Lig3.

Dynamics analysis of selectivity mechanism for inhibitors

As shown in Fig. 1, Lig1 has better PKBα selectivity than Lig2 and Lig3. In the current work, their selectivity toward PKBα rather than PKA is discussed from two aspects. First, considering that the selectivity of an inhibitor is determined by the dissimilarity between the proteins, especially the differences in residues in the binding sites, it is necessary to compare the protein structures of PKBα and PKA. PKA is highly homologous to PKBα, sharing approximately 80 % sequence

Table 1 Binding free energies and its components for the studied inhibitors with proteins[a]

Protein-inhibitor	PKBα-Lig1	PKA-Lig1	PKBα-Lig2	PKA-Lig2	PKBα-Lig3	PKA-Lig3	T211V-Lig1	A230V-Lig1	M281L-Lig1
ΔE_{vdW}	−49.87	−43.57	−48.60	−45.53	−47.95	−47.09	−49.44	−48.60	−47.43
ΔE_{ele}	−202.91	−90.97	−184.11	−100.28	−151.85	−83.22	−142.01	−171.84	−189.82
$\Delta G_{nonpol,\ sol}$	−35.41	−29.79	−32.87	−30.55	−31.84	−30.56	−34.56	−34.08	−34.59
$\Delta G_{ele,\ sol\ (PB)}$	222.51	120.73	202.68	127.12	177.25	113.37	164.63	195.24	204.48
$\Delta G_{ele,\ sol\ (GB)}$	208.67	105.07	189.27	111.60	164.32	102.57	153.29	179.74	191.67
$\Delta E_{vdW}+\Delta G_{nonpol,sol}$	−85.28	−73.36	−81.47	−76.08	−79.79	−77.65	−84.00	−82.68	−82.02
$\Delta E_{ele}+\Delta G_{ele,sol\ (PB)}$	19.60	29.76	18.57	26.84	25.40	30.15	22.62	23.40	14.66
$\Delta E_{ele}+\Delta G_{ele,sol\ (GB)}$	5.76	14.10	5.16	11.32	12.47	19.35	11.28	7.90	1.85
$T\Delta S$	−18.03	−18.96	−25.11	−20.56	−24.81	−24.20	−22.70	−24.98	−19.57
$\Delta G_{pred\ (PB)}$	−47.65	−24.64	−37.79	−28.68	−29.58	−23.30	−38.68	−34.30	−47.79
$\Delta G_{pred\ (GB)}$	−61.49	−40.30	−51.20	−44.20	−42.51	−34.10	−50.02	−49.80	−60.60
$IC_{50\ (nM)}$ [b]	0.5	450	3.3	131.3	7.8	938.3	–	–	–
ΔG_{exp} [c]	−12.75	−8.70	−11.63	−9.44	−11.12	−8.26	–	–	–

[a] All energies are in kcal·mol^{-1}; the MM-PB(GB)SA calculated binding free energy $\Delta G_{pred}=\Delta E_{vdW}+\Delta G_{nonpol,sol}+\Delta E_{ele}+\Delta G_{ele,sol}$ - $T\Delta S$. [b] The IC_{50} values of Lig1, Lig2, and Lig3 were taken from reference [7]. [c] The experimental binding free energy $\Delta G_{exp}\approx -RT\ \ln IC_{50}$

identity within the ATP binding site. There are only three different residues within the clefts of the ATP binding sites of PKBα (Thr211, Ala230 and Met281) and PKA (Val104, Val123, Leu173) [38]. By comparing the MD-simulated representative snapshots of complexes of Lig1 binding to PKBα and three PKBα mutants (Fig. 3a, g, h and i), it is found that the *in silico* site mutation at Thr211, Ala230 and Met281, respectively, of PKBα would not induce the change of binding modes of Lig1. As illustrated in Fig. 3, inhibitors Lig1, Lig2, and Lig3 undergo similar interactions with PKBα and PKA. For example, the nitrogen atom in pyrrolo[2,3-*d*]pyrimidine ring of each inhibitor acts as hydrogen bond acceptors to form hydrogen bonds with the oxygen atoms in the backbone of Ala230 (PKBα) and Val123 (PKA), respectively. The NH group in pyrrolo[2,3-*d*]pyrimidine ring of each inhibitor acts as hydrogen bond donors to form hydrogen bonds with Glu228 of PKBα and Glu121 of PKA, respectively. In addition, the C-12 substituted primary amine group on pyrrolidine ring of each inhibitor become hydrogen bond donor to make hydrogen bonds with Glu234 (PKBα), Glu127 (PKA).

By comparing the MD-simulated representative snapshots of complexes of PKBα with three inhibitors, it is found that the inhibitors have similar interactions in PKBα (Fig. 3a, c and e). In relative to PKA and three PKBα mutants, there are significant movements of the residues (Thr291 and Asp292 of PKBα mutants, Thr183 and Asp184 of PKA) away from the inhibitors (Fig. 3b, d and f, i). In PKA, the side-chain carboxyl group of Asp184 even has a similar trend to rotate 90° away from the inhibitors both in the initial structures and MD results. The rotation caused the disruption of the hydrogen bond between the side-chain carboxyl group of Asp184 in PKA and the NH group of *N*-methylbenzamide group of the inhibitors. On the other hand, the structural alignment of PKBα and PKA indicates that the side chains of Val104, Val123, Leu173 in PKA form a narrower cavity than that enveloped by side chains of Thr211, Ala230 and Met281 in PKBα. To describe the frame of active site, four atoms in the backbone around the inhibitor were chosen as the key points, including a nitrogen atom of Ala230 and three oxygen atoms of Glu228, Glu234, and Asp292 (Fig. 4). The distances between each pair of points were measured to observe the mutational effect on the frame of active site. As shown in Fig. 5, the site mutation causes significant changes in the frame of active site. All these data suggest that these three residues are important for maintaining the shape of active site which is essential for the selectivity of PKBα inhibitor.

The hydrogen-bond interactions and free energy decomposition were further analyzed to characterize the detailed interactions between inhibitors and residues based on the above

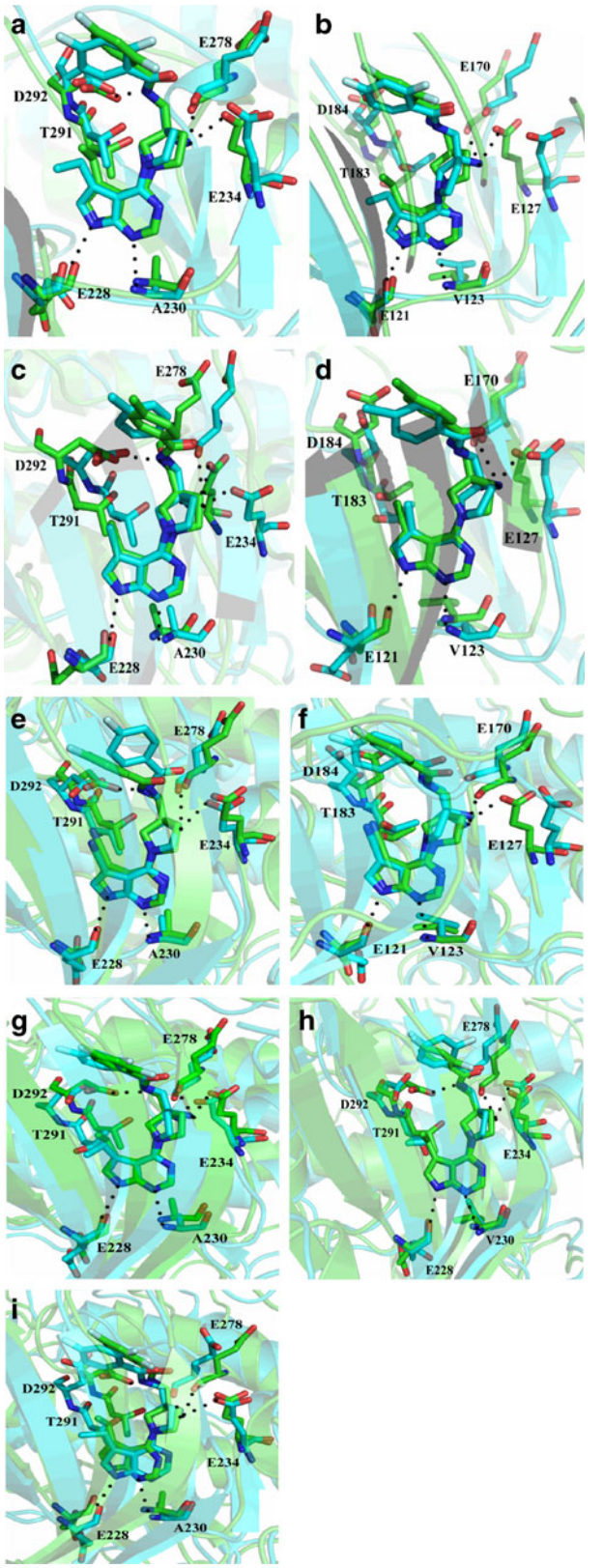

Fig. 3 Structure comparison between initial (green) and representative snapshot from MD (cyan) of: (**a**) PKBα-Lig1, (**b**) PKA-Lig1, (**c**) PKBα-Lig2, (**d**) PKA-Lig2, (**e**) PKBα-Lig3, (**f**) PKA-Lig3, (**g**) T211V-Lig1, (**h**) A230V-Lig**1**, (**i**) M281L-Lig1

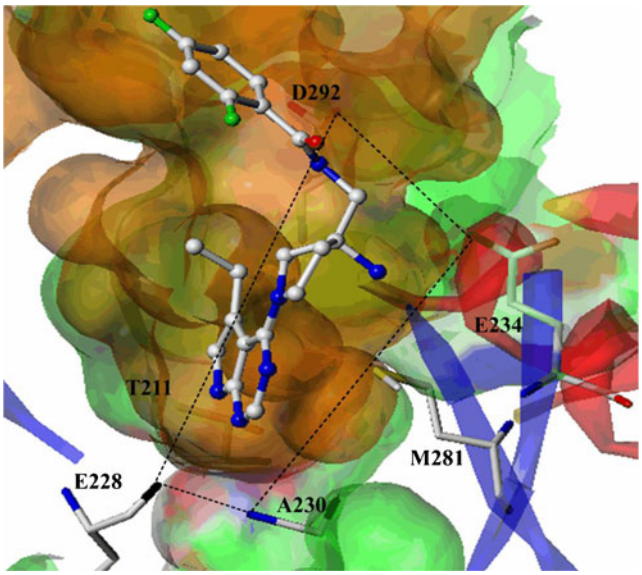

Fig. 4 Comparison of the inhibitor-binding pockets, depicted by solvent accessible surfaces, in the X-ray structures of PKBα (green) and PKA (orange). Dash-line linked four atoms from four key residues (PKBα numbering) were applied to define the frame of active site

work, which will provide more quantitative information. They are investigated and discussed in the following sections.

Comparison of the binding modes of Lig1 in complexes PKBα-Lig1, mutants-Lig1 and PKA-Lig1 As indicated in Fig. 6a, c and e, the interactions between inhibitors and the residues Leu156, Gly157, Val164, Ala177, Met227, Glu228, Tyr229, Ala230, Glu234, Glu278, Met281, Thr291, and Phe438 of PKBα are the most favorable dominant contributions to the binding of the three ligands, but the unfavorable electrostatic interactions between Lig1 or Lig2 and the residues Lys179 and Asp292 of PKBα are also found. The major

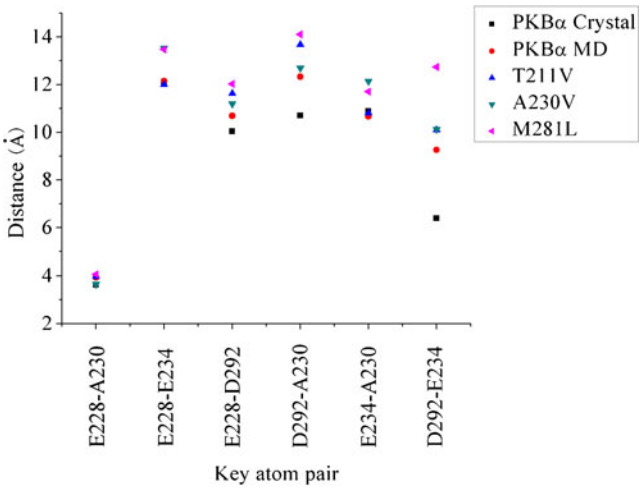

Fig. 5 The atom-to-atom distances between the atoms in backbone at the key positions

favorable energy contributions arise predominantly from the residues Leu156, Gly157, Val164, Ala177, Lys179, Glu228, Tyr229, Ala230 (or Val230 of PKBα mutant A230V), Glu234, Met281 (or Leu281 of PKBα mutant M230L), Thr291 and Phe438 of three PKBα mutants. Lys179 produces the unfavorable electrostatic interaction to the binding of three ligands with PKBα mutants (Fig. 6g, h and i). Residues Leu49, Gly50, Val57, Ala70, Lys72, Glu121, Tyr122, Val123, Glu127, Leu173 and Thr183 of PKA make the major favorable energy contributions to the inhibitors binding to PKA. The binding of the three ligands with PKA are counteracted by the unfavorable electrostatic interactions of inhibitors Lig1, Lig2, and Lig3 with Lys72 (Fig. 6b, d and f). Special attention was paid to those residues with relatively large differences of the binding free energies. Both C-12 substituted primary amine group and the NH group of C-12 substituted *N*-methylbenzamide group on pyrrolidine ring of Lig1 could make hydrogen bonds with Glu234 and Glu278 of PKBα, respectively. These favorable interactions are supported by the per-residue energy decomposition. As shown in Fig. 6a and b, the energy contributions are −7.27±0.02 kcal·mol^{-1} and −2.47±0.02 kcal·mol^{-1} for the residues of Glu234 and Glu278 of PKBα, while the energy contributions arise only from Glu127 (−0.97±0.02 kcal·mol^{-1}) of PKA because of the rotations of the side-chain carboxyl groups of Glu170 (−0.21±0.02 kcal·mol^{-1}) and Asp184 (−0.18±0.02 kcal·mol^{-1}). Compared with Lig1 binding to PKBα mutants, the residue Glu278 of PKBα makes a stronger interaction with C-12 substituted primary amine group of Lig1 (−2.47±0.02 kcal·mol^{-1}) than those in both mutants of T211V (−0.17±0.02 kcal·mol^{-1}) and A230V (−0.47±0.02 kcal·mol^{-1}), while it has weaker interaction than that in M281L (−4.08±0.02 kcal·mol^{-1}). The residue Glu234 forms a stronger hydrogen bond interaction with C-12 substituted primary amine group of Lig1 (−7.27±0.02 kcal·mol^{-1}) in PKBα than that in all three PKBα mutants, T211V (−6.22±0.02 kcal·mol^{-1}), A230V (−6.17±0.02 kcal·mol^{-1}), and M281L (−5.31±0.02 kcal·mol^{-1}) (Fig. 6).

The above results are supported by the H-bond analysis. We applied the ptraj program in Amber 11 [22] to calculate the H-bond length and angle of the corresponding hydrogen bonds. As shown in Table 2, the NH group and N atom in pyrrolo[2,3-*d*]pyrimidine ring of Lig1 form stable hydrogen bonds with Glu228, Ala230 in PKBα (>99 % occupancy), PKBα mutants (>99 % occupancy), and Glu121, Val123 in PKA (>99 % occupancy). The NH group of C-12 substituted *N*-methylbenzamide group and primary amine group also form hydrogen bond interactions with Asp292 (57 % occupancy) and Glu278 (54 % occupancy) of PKBα. Both side-chain carboxyl O atoms of Asp292 could make hydrogen bonds with NH group of C-12 substituted *N*-methylbenzamide group of Lig1. In PKA, the C-12 substituted primary amine group of Lig1 forms hydrogen bond interactions with Glu127 (37 %

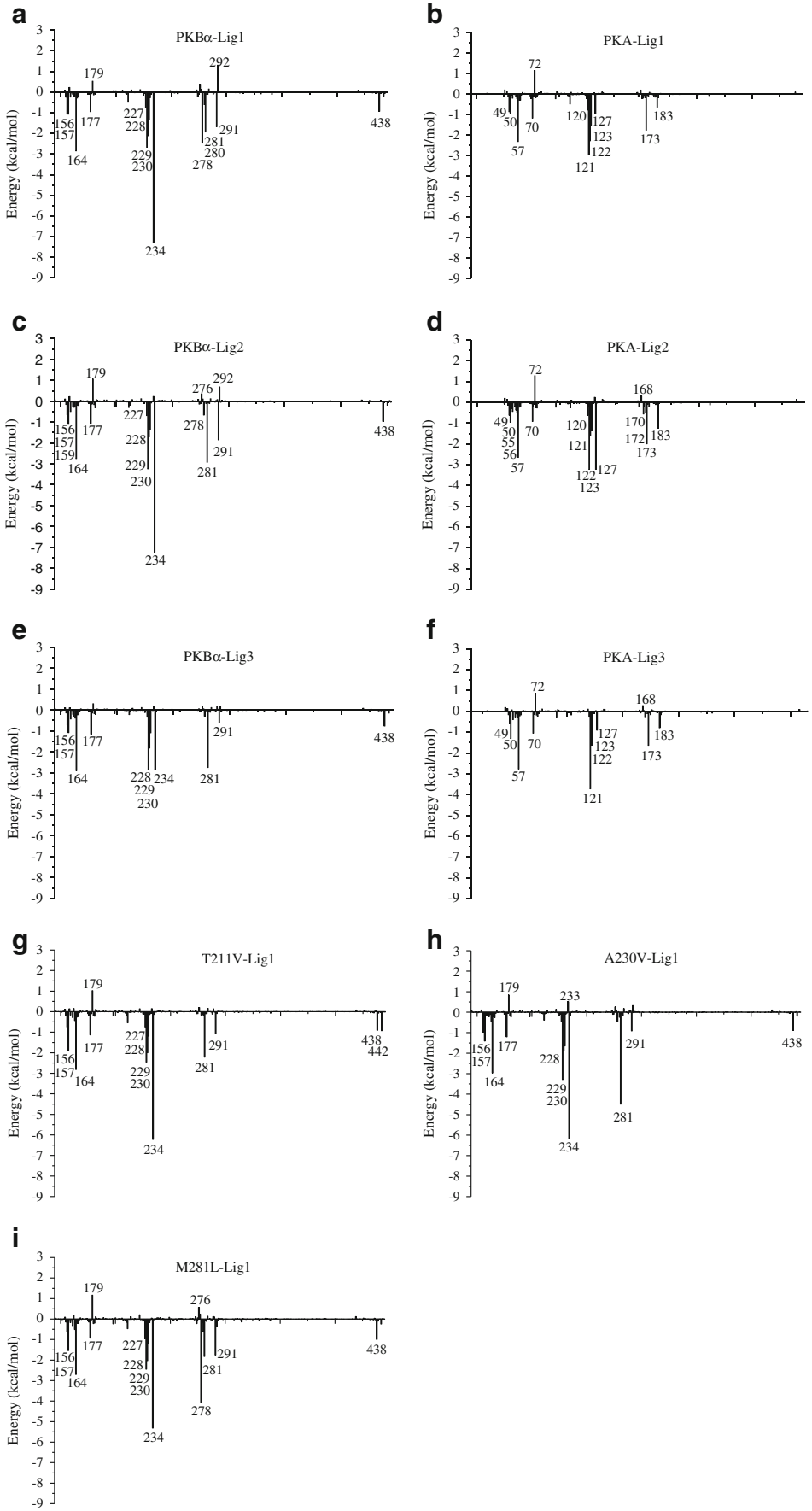

Fig. 6 Inhibitor-residue interaction spectra of: (**a**) PKBα-Lig1, (**b**) PKA-Lig1, (**c**) PKBα-Lig2, (**d**) PKA-Lig2, (**e**) PKBα-Lig3, (**f**) PKA-Lig3, (**g**) T211V-Lig1, (**h**) A230V-Lig1, (**i**) M281L-Lig1

Table 2 Hydrogen bonds analysis from MD[a]

System	Donor	Acceptor	Occupancy(%)[b]	Distance(Å)[c]	Angle(°)[d]
PKBα-Lig1	Ala230 N-H	Lig1 N1	100	3.16±0.24	160.13±11.68
	Lig1 N8-H	Glu228 O	100	2.88±0.16	160.08±10.54
	Lig1 N16-H	Glu292 OD1	58	3.64±0.73	146.26±14.00
	Lig1 N16-H	Glu292 OD2	57	4.48±0.38	155.40±15.00
	Lig1 N25-H	Glu278 O	55	4.37±0.59	133.45±9.78
PKA-Lig1	Val123 N-H	Lig1 N1	96	3.26±0.24	152.47±14.47
	Lig1 N8-H	Glu121 O	100	2.86±0.13	157.51±10.72
	Lig1 N25-H	Glu127 OE1	38	3.09±0.70	156.31±14.73
	Lig1 N25-H	Glu170 O	35	4.64±0.24	134.26±9.77
PKBα-Lig2	Ala230 N-H	Lig2 N1	100	3.13±0.19	161.13±10.97
PKA-Lig2	Val123 N-H	Lig2 N1	99	3.26±0.27	157.82±12.45
PKBα-Lig3	Ala230 N-H	Lig3 N1	98	3.12±0.16	155.64±12.99
	Lig3 N8-H	Glu228 O	100	2.87±0.13	157.54±10.54
	Lig3 N25-H	Glu234 OE1	31	2.95±0.53	152.98±12.64
PKA-Lig3	Val123 N-H	Lig3 N1	96	3.26±0.20	153.84±13.68
	Lig3 N8-H	Glu121 O	100	2.84±0.12	156.37±10.78
	Lig3 N16-H	Asp184 OD1	34	4.04±0.76	150.62±13.73
	Lig3 N16-H	Asp184 OD2	30	4.08±0.71	144.76±13.13
T211V-Lig1	Ala230 N-H	Lig1 N1	98	3.13±0.17	157.18±13.17
	Lig1 N8-H	Glu228 O	100	2.86±0.12	159.31±10.28
A230V-Lig1	Ala230 N-H	Lig1 N1	99	3.18±0.20	159.54±11.98
	Lig1 N8-H	Glu228 O	100	2.85±0.11	160.97±9.88
	Lig1 N16-H	Asp292 OD2	32	4.53±0.43	146.23±13.75
M281L-Lig1	Ala230 N-H	Lig1 N1	97	3.35±0.27	155.42±13.92
	Lig1 N8-H7	Glu228 O	100	2.83±0.11	158.85±10.71
	Lig1 N25-H	Glu278 O	81	2.84±0.12	155.28±11.25

[a] The listed donor and acceptor pairs satisfy the criteria (H-bond length less than 5 Å and H-bond angle in the range of 120 ° ~180 °) for the hydrogen bond over 30.0 % of the time during the 16 ns of MD simulation. [b] Occupancy is the percentage of H-bond formed during the investigated time period. [c] The average distance with standard error (SE=standard deviation/$N^{1/2}$) between H-bond acceptor and proton on H-bond donor in the investigated time period. [d] The average H-bond angle with standard error (SE=standard deviation/$N^{1/2}$) in the investigated time period

occupancy) and Glu170 (35 % occupancy). The NH group of C-12 substituted *N*-methylbenzamide group of Lig1 forms a hydrogen bond with Asp292 (31.8 % occupancy) of PKBα mutant A230V. The C-12 substituted primary amine group of Lig1 forms a hydrogen bond with Glu278 (81.4 % occupancy) of M281L. Also, Lig1 binds deeply into the active pocket of PKBα, creating favorably hydrophobic interactions with more residues than that with PKA. The hydrophobic interaction of C-6 ethyl-substituted pyrrolo[2,3-*d*]pyrimidine ring of Lig1 with residues Thr291 (−1.67± 0.02 kcal·mol^{-1}) and Phe438 (−0.93±0.02 kcal·mol^{-1}) contribute energetically more to PKBα than Thr183 (−0.65±0.02 kcal·mol^{-1}) and Phe185 (−0.02± 0.02 kcal·mol^{-1}) to PKA. The hydrophobic interaction of C-6 substituted ethyl group on pyrrolo[2,3-*d*]pyrimidine ring with residue Thr291 (−1.67±0.02 kcal·mol^{-1}) also contributes energetically more to PKBα than that in T211V (−1.07±0.02 kcal·mol^{-1}) and A230V (−0.91± 0.02 kcal·mol^{-1}), except for M281L (−1.75±0.02 kcal·mol^{-1}). As illustrated in Fig. 7 and 8, the contributions of van der Waals and nonpolar solvation energies of Glu278, Thr291, Asp292 were responsible for the differences between PKBα-Lig1 and T211V-Lig1, A230V-Lig1, while only the contributions of van der Waals and nonpolar solvation energies of Asp292 were responsible for the differences between PKBα-Lig1 and M281L-Lig1 (Fig. 7a). As shown in Fig. 8a, the residues Gly157, Lys163, Val164, Met227, Glu278, Met281, Thr291, Asp292, and Phe438 make more contributions of van der Waals and nonpolar solvation energies to PKBα than the residues Gly50, Arg56, Val57, Met120, Asn171, Ile174, Asp184, Phe185, and Glu331 to PKA. The different van der Waals and nonpolar solvation energies were responsible for the differences between PKBα-Lig1 and PKA-Lig1 (Fig. 8a). The total electrostatic energies of Glu228, Glu234 and Glu278 yield the energetic differences between PKBα-Lig1 and the mutants-Lig1 (Fig. 7b). The total electrostatic energies of Glu234 (Glu127 in PKA) and Glu278 (Asn171 in PKA) of PKBα yield the energetic differences between PKBα-Lig1 and PKA-Lig1 (Fig. 8b).

As illustrated in Fig. 6a and b, *o*, *p*- difloro substitutions on the phenyl ring of Lig1 have little impact on the selectivity of the inhibitor. The C-6 substituted ethyl group on pyrrolo[2,3-

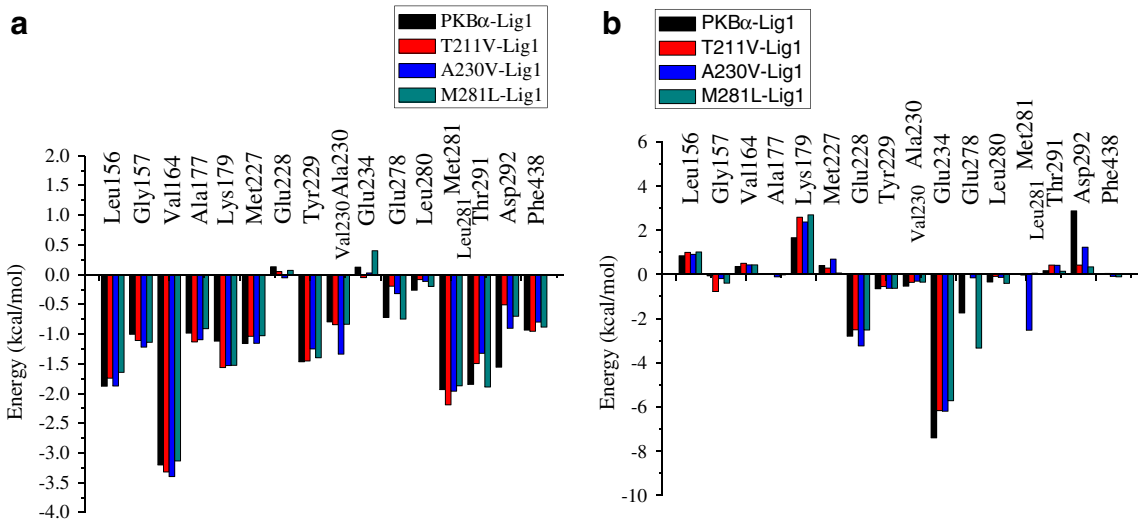

Fig. 7 Comparison of per-residue energy decomposition for key residues for four systems: (**a**) the sums of vdW and nonpolar solvation energy ($\Delta G_{vdW}+\Delta G_{nonpol,\ sol}$) of PKBα-Lig1, T211V-Lig1, A230V-Lig1 and M281L-Lig1, (**b**) the sums of electrostatic and polar solvation energy ($\Delta G_{ele}+\Delta G_{ele,sol}$) of PKBα-Lig1, T211V-Lig1, A230V-Lig1 and M281L-Lig1

d]pyrimidine ring of Lig1 more favorably interacts with Thr291 of PKBα than Thr183 of PKA. Due to the narrow cavity in PKA and the mutants, C-12 substituted *N*-methylbenzamide group on pyrrolidine ring is more tolerable in PKBα, which indicates that the C-12 substituted primary amine group and the NH group of C-12 substituted *N*-methylbenzamide group on pyrrolidine ring of Lig1 can form stronger hydrogen bonds with the side chain carboxyl O atoms of Glu234, Glu278, and Asp292 of PKBα than the corresponding residues of PKA and three PKBα mutants. All these data show the selective mechanism of Lig1 for PKBα over PKA (PKA selectivity ratio=900).

Comparison of the binding modes of Lig2 in complexes PKBα-Lig2 and PKA-Lig2 As illustrated in Fig. 6c and d, the energy contribution of Glu234 (-7.23 ± 0.02 kcal·mol^{-1}) in PKBα-Lig2 contributes twice more than that of Glu127 (-3.23 ± 0.02 kcal·mol^{-1}) in PKA-Lig2. It can be seen that Lig2 forms stable hydrogen bonds only with Ala230 in PKBα (99 % occupancy) and Val123 in PKA (99 % occupancy) in Table 2. Also, there are hydrophobic interactions of C-6 cyano-substituted pyrrolo[2,3-*d*]pyrimidine ring in Lig2 with residues Met281 (-2.92 ± 0.02 kcal·mol^{-1}), Thr291 (-1.85 ± 0.02 kcal·mol^{-1}) and Phe438 (-0.96 ± 0.02 kcal·mol^{-1}) in PKBα, but with two residues Leu173 (-2.00 ± 0.02 kcal·

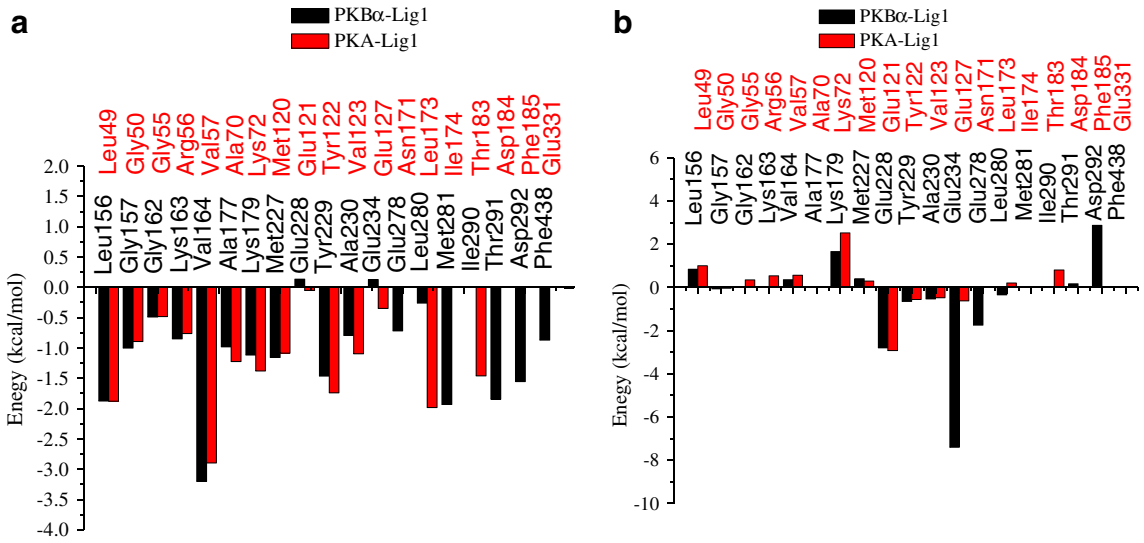

Fig. 8 Comparison of per-residue energy decomposition for key residues for Lig1-protein systems: (**a**) the sums of vdW and nonpolar solvation energy ($\Delta G_{vdW}+\Delta G_{nonpol,\ sol}$) of Lig1-PKBα (black) and Lig1-PKA (red), (**b**) the sums of electrostatic and polar solvation energy ($\Delta G_{ele}+\Delta G_{ele,\ sol}$) of Lig1-PKBα (black) and Lig1-PKA (red)

mol^{-1}) and Thr183 (−1.25±0.02 kcal·mol^{-1}) in PKA (Fig. 6c and d). As shown in Fig. 9a, the distinct differences of the van der Waals and nonpolar solvation energies can be identified on the residues Val164, Ala177, Lys179, Met227, Tyr229, Glu278, Met281, Thr291, Asp292, and Phe438 of PKBα and the residues Val57, Ala70, Lys72, Met120, Tyr122, Asn171, Ile174, Asp184, Phe185, and Glu331 of PKA. The different van der Waals and nonpolar solvation energies make major contributions to the differences between PKBα-Lig2 and PKA-Lig2. Furthermore, the residues Glu228, Tyr229, Ala230, Glu234, Glu278, and Met281 of PKBα make more contributions to the total electrostatic energies to the binding inhibitor than the residues Glu121, Tyr122, Val123, Glu127, Asn171 and Ile174 of PKA. These different total electrostatic energies yield the differences for PKBα-Lig2 and PKA-Lig2 (Fig. 9b). According to the above results, *p*-F substitution on phenyl ring of Lig2 still has little impact on the selectivity of the inhibitor. C-6 substituted cyano group on pyrrolo[2,3-*d*]pyrimidine ring of Lig2 more favorably interacts with Thr291 in PKBα than Thr183 in PKA. The C-12 substituted primary amine group and the NH group of C-12 substituted *N*-methylbenzamide group on pyrrolidine ring also makes Lig2 form stronger hydrogen bonds with the side chain carboxyl O atoms of Glu234, Asp292 than the corresponding residues of Lig2 in PKA. They are responsible for the selectivity of Lig2 for PKBα over PKA (PKA selectivity ratio=39.8). In PKA, the C-6 substituted cyano group of Lig2 (−1.25±0.02 kcal·mol^{-1}) more favorably interacts with Thr183 than the C-6 substituted ethyl group of Lig1 (−0.21 ±0.02 kcal·mol^{-1}), which leads to the better activity of Lig2 in PKA and the lower selectivity of Lig2.

Comparison of binding modes of Lig3 in complexes PKBα-Lig3 and PKA-Lig3 As illustrated in Fig. 6e and f, the favorable hydrogen bond interaction shows that the energy contribution of Glu234 is −2.83±0.02 kcal·mol^{-1} in PKBα while the energy contribution of Glu127 is only −0.90±0.02 kcal·mol^{-1} in PKA. However, the energy contribution of Glu121 (−3.72±0.02 kcal·mol^{-1}) in PKA contributes more than that of Glu228 (−2.84±0.02 kcal·mol^{-1}) in PKBα. These are also supported by the hydrogen bond analyses. As shown by Table 2, NH group and N atom in pyrrolo[2,3-*d*]pyrimidine ring of Lig3 form stable hydrogen bonds with Glu228 and Ala230 of PKBα (> 99 % occupancy), Glu121 and Val123 of PKA (> 99 % occupancy). In addition, there is a hydrogen bond interaction between Glu234 (PKBα) with the C-12 substituted primary amine group on pyrrolidine ring of Lig3 (31 % occupancy). The hydrophobic interaction of C-6 substituted chloro group of Lig3 with residue Thr291 (−0.59 ±0.02 kcal·mol^{-1}) contributes energetically to PKBα less than Thr183 (−0.79±0.02 kcal·mol^{-1}) to PKA. However, there are another two hydrophobic interactions presented between C-6 chloro-substituted pyrrolo[2,3-*d*]pyrimidine ring of Lig3 and residues Met281 (−2.75±0.02 kcal·mol^{-1}) and Phe438 (−0.76±0.02 kcal·mol^{-1}) of PKBα. In PKA, only Leu173 (−1.63±0.02 kcal·mol^{-1}) contributes to PKA. By analyzing the van der Waals and nonpolar solvation energies of residues Val164, Lys179, Tyr229, Ala230, Met281, Thr291, Asp292 and Phe438 of PKBα, and residues Val57, Lys72, Tyr122, Val123, Ile174, Asp184, Phe185 and Glu331 of PKA (Fig. 10a), it can be found that the different van der Waals and nonpolar solvation energies were mainly responsible for the differences between PKBα-Lig3 and PKA-Lig3. The differences of total electrostatic energies of residues

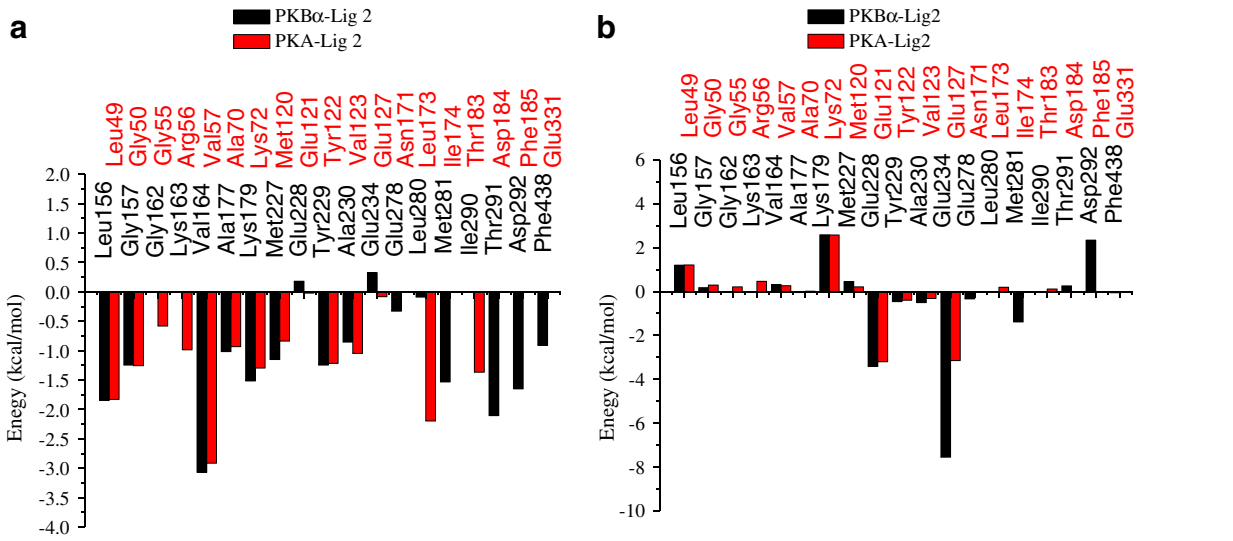

Fig. 9 Comparison of per-residue energy decomposition for key residues for Lig2-protein systems: (**a**) the sum of vdW and nonpolar solvation energy ($\Delta G_{vdW}+\Delta G_{nonpol,\ sol}$) of Lig2-PKBα (black) and Lig2-PKA (red), (**b**) the sums of electrostatic and polar solvation energy ($\Delta G_{ele}+\Delta G_{ele,\ sol}$) of Lig2-PKBα (black) and Lig2-PKA (red)

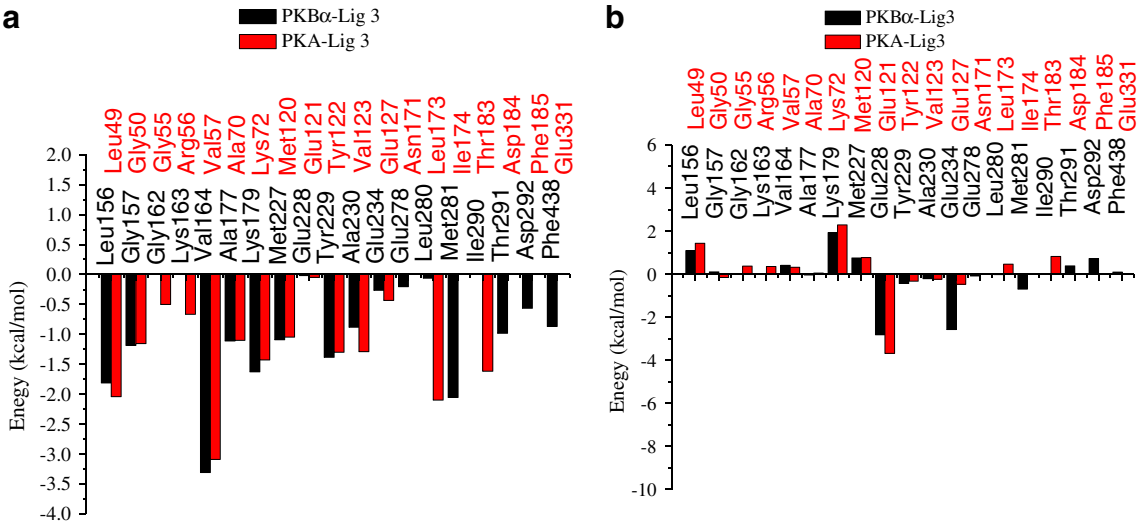

Fig. 10 Comparison of per-residue energy decomposition for key residues for Lig3-binding systems: (**a**) the sums of vdW and nonpolar solvation energy ($\Delta G_{vdW}+\Delta G_{nonpol,\ sol}$) of Lig3-PKBα (black) and Lig3-PKA (red), (**b**) the sums of electrostatic and polar solvation energy ($\Delta G_{ele}+\Delta G_{ele,\ sol}$) of Lig3-PKBα (black) and Lig3-PKA (red)

Glu234, Met281 of PKBα and Glu127, Ile174 of PKA yield the energetic differences for PKBα-Lig3 and PKA-Lig3 (Fig. 10b). Therefore, it is hypothesized that 4-Cl substitution on the phenyl ring of Lig3 has little impact on the selectivity of Lig3. The weak hydrophobic interaction of C-6 substituted chloro group on pyrrolo[2,3-*d*]pyrimidine ring of Lig3 and weak hydrogen-bond interaction of Glu228 suggest that Lig3 has the lowest activity in PKBα. However, Lig3 favorably interacts with Met281, Phe438 of PKBα than the corresponding residues of PKA. The C-12 substituted primary amine group of Lig3 can form stronger hydrogen bonds with the side chanin carboxyl O atoms of Glu234 of PKBα than Lig3 in PKA. The data indicate that Lig3 has better activity in PKBα than in PKA (PKA selectivity ratio=120.3). Leu173 and Thr183 of PKA contribute less to the C-6 substituted chloro group on pyrrolo[2,3-*d*]pyrimidine ring of Lig3 (Leu173: -1.63±0.02 kcal·mol^{-1}; Thr183: -0.79±0.02 kcal·mol^{-1}) than the similar C-6 substituted cyano group of Lig2 (Leu173: -2.00±0.02 kcal·mol^{-1}; Thr183: -1.25±0.02 kcal·mol^{-1}), leading to the lower PKA activity of Lig3 than Lig2. This explains the better selectivity of Lig3 over Lig2.

Above all, we focused on the detailed comparison in interaction features of inhibitors Lig1, Lig2, and Lig3, with different potency and selectivity to PKBα and PKA, to understand the structural requirements of the ligand which enhance the binding affinity. The results are in good agreement with experimental data. All the results we have observed above clearly suggest that the substitutions at the phenyl group of inhibitors have little impact on their selectivity. Hydrophobic interactions of C-6 substituted group on pyrrolo[2,3-*d*]pyrimidine ring such as the ethyl group and hydrogen bond interactions of C-12 substituted groups on pyrrolidine ring such as the amino and amide groups are critical for PKBα selectivity. The work provides a possible effective pharmacophore features for further rational design of PKBα selective inhibitors.

Conclusions

In this study, we applied molecular dynamics (MD) simulations and free energy calculations of inhibitors Lig1, Lig2, and Lig3 binding to PKBα, PKA, and three PKBα mutants (T211V, A230V, M281L), respectively. Detailed perspectives from the protein and ligand viewpoints have been provided regarding the selectivity aspect of Lig1 toward PKBα. The roles of the three key different amino acids (Thr211, Ala230, and Met281 of PKBα, Val104, Val123, and Leu173 of PKA) in determining its selectivity toward PKBα over PKA has been rationally analyzed. The *in silico* mutation results show that point mutations of the residues Thr211, Ala230, and Met281, respectively, of PKBα lead to higher binding free energies and have a big influence on the shape of the active site, which directly affects the conformations of inhibitors and consequently obstructs their hydrogen bonding abilities with the proteins. This indicates that Thr211, Ala230, Met281 of PKBα could lead to the enhanced binding affinity and selectivity of its inhibitor. The mechanism of PKBα selective inhibition was also elucidated through the analysis of the binding modes of inhibitors Lig1, Lig2, and Lig3, respectively, on either PKBα or PKA. Comparing MD simulated interaction modes between PKBα, PKA, and three PKBα mutants (T211V, A230V, M281L) and three inhibitors, it could be

concluded that the C-12 substituted *N*-methylbenzamide group on pyrrolidine ring is more tolerable by PKBα. In comparison to the ligand-protein complexes of inhibitors Lig2 and Lig3, there are two components that lead to the increased selectivity toward complexes of Lig1. These include ethyl group at the 6-position on pyrrolo[2,3-*d*]pyrimidine ring which more preferably interacts with hydrophobic portions of the side chain of Thr291 and the strong hydrogen bonds formed between the carboxyl O atoms of Glu234, Glu278, and Asp292 and the C-12 substituted primary amine group and the NH group of C-12 substituted *N*-methylbenzamide group on pyrrolidine ring. So these observations provide a better structural understanding of the mechanism of PKBα selective inhibition. They are also expected to provide a basis for further rational design of new potent inhibitors to PKBα.

Acknowledgments The authors are thankful to the College of Pharmaceutical Sciences, Zhejiang University for providing necessary facilities.

References

1. Barnett SF, Bilodeau MT, Lindsley CW (2005) The Akt/PKB family of protein kinases: a review of small molecule inhibitors and progress towards target validation. Curr Top Med 5:109–125
2. Lindsley CW, Barnett SF, Yaroschak M, Bilodeau MT, Layton ME (2007) Recent progress in the development of ATP-competitive and allosteric Akt kinase inhibitors. Curr Top Med 7: 1349–1363
3. Fayard E, Tintignac LA, Baudry A, Hemmings BA (2005) Protein kinase B/Akt at a glance. J Cell Sci 118(24):5675–5678
4. Li Q, Zhu G-D (2002) Targeting serine/threonine protein kinase B/Akt and cell-cycle checkpoint kinases for treating cancer. Curr Top Med 2(9):939–971
5. Cheng GZ, Park S, Shu S, He L, Kong W, Zhang W, Yuan Z, Wang L-H, Cheng JQ (2008) Advances of AKT pathway in human oncogenesis and as a target for anti-cancer drug discovery. Curr Cancer Drug Tar 8:2–6
6. Thakur DS, Kumar P, Kumar P, Lal C (2010) Akt: a new approach for cancer treatment. Int J Pharm Sci Res 1(suppl8):29–36
7. Freeman-Cook KD, Autry C, Borzillo G, Gordon D, Barbacci-Tobin E, Bernardo V, Briere D, Clark T, Corbett M, Jakubczak J, Kakar S, Knauth E, Lippa B, Luzzio MJ, Mansour M, Martinelli G, Marx M, Nelson K, Pandit J, Rajamohan F, Robinson S, Subramanyam C, Wei L, Wythes M, Morris J (2010) Design of selective, ATP-competitive inhibitors of Akt. J Med Chem 53:4615–4622
8. Rhodes N, Heerding DA, Duckett DR, Eberwein DJ, Knick VB, Lansing TJ, McConnell RT, Gilmer TM, Zhang S-Y, Robell K, Kahana JA, Geske RS, Kleymenova EV, Choudhry AE, Lai Z, Leber JD, Minthorn EA, Strum SL, Wood ER, Huang PS, Copeland RA, Kumar R (2008) Characterization of an Akt kinase inhibitor with potent pharmacodynamic and antitumor activity. Cancer Res 68(7): 2366–2374
9. Blake JF, Xu R, Bencsik JR, Xiao D, Kallan NC, Schlachter S, Mitchell IS, Spencer KL, Banka AL, Wallace EM, Gloor SL, Martinson M, Woessner RD, Vigers GPA, Brandhuber BJ, Liang J, Safina BS, Li J, Zhang B, Chabot C, Do S, Lee L, Oeh J, Sampath D, Lee BB, Lin K, Liederer BM, Skelton NJ (2012) Discovery and preclinical pharmacology of a selective ATP competitive Akt inhibitor (GDC-0068) for the treatment of human tumors. J Med Chem 55(18):8110–8127
10. Xu R, Banka A, Blake JF, Mitchell IS, Wallace EM, Bencsik JR, Kallan NC, Spencer KL, Gloor SL, Martinson M, Risom T, Gross SD, Morales TH, Wu W-I, Vigers GPA, Brandhuber BJ, Skelton NJ (2011) Discovery of spirocyclic sulfonamides as potent Akt inhibitors with exquisite selectivity against PKA. Bioorg Med Chem Lett 21:2335–2340
11. Kallan NC, Spencer KL, Blake JF, Xu R, Heizer J, Bencsik JR, Mitchell IS, Gloor SL, Martinson M, Risom T, Gross SD, Morales TH, Wu W-I, Vigers GPA, Brandhuber BJ, Skelton NJ (2011) Discovery and SAR of spirochromane Akt inhibitors. Bioorg Med Chem Lett 21:2410–2414
12. Bencsik JR, Xiao D, Blake JF, Kallan NC, Mitchell IS, Spencer KL, Xu R, Gloor SL, Martinson M, Risom T, Woessner RD, Dizon F, Wu W-I, Vigers GPA, Brandhuber BJ, Skelton NJ, Prior WW, Murray LJ (2010) Discovery of dihydrothieno- and dihydrofuropyrimidines as potent pan Akt inhibitors. Bioorg Med Chem Lett 20:7037–7041
13. Mascarenhas NM, Bhattacharyya D, Ghoshal N (2010) Why pyridine containing pyrido[2,3-d]pyrimidin-7-ones selectively inhibit CDK4 than CDK2: Insights from molecular dynamics simulation. J Mol Graph Mod 28:695–706
14. Yang Y, Qin J, Liu H, Yao X (2011) Molecular dynamics simulation, free energy calculation and structure-based 3D-QSAR studies of B-RAF kinase inhibitors. J Chem Inf Model 51:680–692
15. Yang Y, Shen Y, Liu H, Yao X (2011) Molecular dynamics simulation and free energy calculation studies of the binding mechanism of allostericinhibitors with p38α MAP kinase. J Chem Inf Model 51: 3235–3246
16. Chen Q, Cui W, Cheng Y, Zhang F, Ji M (2011) Studying the mechanism that enables paullones to selectively inhibit glycogen synthase kinase 3 rather than cyclin-dependent kinase 5 by molecular dynamics simulations and free-energy calculations. J Mol Model 17: 795–803
17. Kollman PA, Massova I, Reyes C, Kuhn B, Huo S, Chong L, Lee M, Lee T, Duan Y, Wang W, Donini O, Cieplak P, Srinivasan J, Case DA, Cheatham TE (2000) Calculating structures and free energies of complex molecules: combining molecular mechanics and continuum models. Acc Chem Res 33:889–897
18. Gohlke H, Kiel C, Case DA (2003) Insights into protein-protein binding by binding free energy calculation and free energy decomposition for the Ras-Raf and Ras-RalGDS complexes. J Mol Biol 330:891–913
19. Wong S, Amaro RE, McCammon JA (2009) MM-PBSA captures key role of intercalating water molecules at a protein-protein interface. J Chem Theory Comput 5:422–429
20. Jiao D, Zhang J, Duke RE, Li G, Schnieders MJ, Ren P (2009) Trypsin-ligand binding free energies from explicit and implicit solvent simulations with polarizable potential. J Comput Chem 30(11): 1701–1711
21. Jain AN (2007) Surflex-Dock 2.1: robust performance from ligand energetic modeling, ring flexibility, and knowledge-based search. J Comput Aided Mol Des 21:281–306
22. Case DA, Darden TA, Cheatham TE, Simmerling CL, Wang J, Duke RE, Luo R, Walker RC, Zhang W, Merz KM, Roberts B, Wang B, Hayik S, Roitberg A, Seabra G, Kolossváry I, Wong KF, Paesani F, Vanicek J, Liu J, Wu X, Brozell SR, Steinbrecher T, Gohlke H, Cai Q, Ye X, Wang J, Hsieh MJ, Cui G, Roe DR, Mathews DH, Seetin MG, Sagui C, Babin V, Luchko T, Gusarov S, Kovalenko A, Kollman P (2010) AMBER 2011 University of California, San Francisco
23. Jorgensen W, Chandrasekhar J, Madura J, Impey R, Klein M (1983) Comparison of simple potential functions for simulating liquid water. J Chem Phys 79:926–935
24. Duan Y, Wu C, Chowdhury S, Lee MC, Xiong G, Zhang W, Yang R, Cieplak P, Luo R, Lee T, Caldwell J, Wang J, Kollman P (2003) A point-charge force field for molecular mechanics simulations of

proteins based on condensed-phase quantum mechanical calculations. J Comput Chem 24:1999–2012
25. Wang J, Wolf RM, Caldwell JW, Kollman PA, Case DA (2004) Development and testing of a general amber force field. J Comput Chem 25:1157–1174
26. Darden T, York D, Pedersen L (1993) Particle mesh Ewald: An $N\cdot\log(N)$ method for Ewald sums in large systems. J Chem Phys 98: 10089–10092
27. Berendsen HJC, Postma JPM, Gunsteren WFV, DiNola A, Haak JR (1984) Molecular dynamics with coupling to an external bath. J Chem Phys 81:3684–3690
28. Ryckaert J-P, Ciccotti G, Berendsen HJC (1977) Numerical integration of the cartesian equations of motion of a system with constraints: molecular dynamics of n-alkanes. J Comput Phys 23(3):327–341
29. Case DA, Darden TA, Cheatham TE, Simmerling CL, Wang J, Duke RE, Luo R, Walker RC, Zhang W, Merz KM, Roberts B, Wang B, Hayik S, Roitberg A, Seabra G, Kolossváry I, Wong KF, Paesani F, Vanicek J, Liu J, Wu X, Brozell SR, Steinbrecher T, Gohlke H, Cai Q, Ye X, Wang J, Hsieh MJ, Cui G, Roe DR, Mathews DH, Seetin MG, Sagui C, Babin V, Luchko T, Gusarov S, Kovalenko A, Kollman P.(2012) AMBER 2012 University of California, San Francisco
30. Rocchia W, Alexov E, Honig B (2001) Extending the applicability of the nonlinear Poisson-Boltzmann equation: multiple dielectric constants and multivalent ions. J Phys Chem B 105:6507–6514
31. Onufriev A, Bashford D, Case DA (2004) Exploring protein native states and large-scale conformational changes with a modified generalized Born model. Proteins Struct, Funct, Bioinform 55(2): 383–394
32. Weiser J, Shenkin PS, Still WC (1999) Approximate atomic surfaces from linear combinations of pairwise overlaps (LCPO). J Comput Chem 20:217–230
33. Li Y, Zhang J, He D, Liang Q, Wang Y (2012) Characterization of molecular recognition of Phosphoinositide-3-kinase α inhibitor through molecular dynamics simulation. J Mol Model 18:1907–1916
34. Lu S-Y, Jiang Y-J, Zou J-W, Wu T-X (2012) Effect of double mutations K214/A–E215/Q of FRATide on GSK3β: insights from molecular dynamics simulation and normal mode analysis. Amino Acids 43:267–277
35. Bayly CI, Cieplak P, Cornell WD, Kollman PA (1993) A well-behaved electrostatic potential based method using charge restraints for deriving atomic charges: the RESP model. J Phys Chem 97: 10269–10280
36. Rizzo RC, Tirado-Rives J, Jorgensen WL (2001) Estimation of binding affinities for HEPT and nevirapine analogues with HIV-1 reverse transcriptase via Monte Carlo simulations. J Med Chem 44:145–154
37. Alexey O, Donald B, David AC (2004) Exploring protein native states and large-scale conformational changes with a modified generalized born model. Proteins 55:383–394
38. Davies TG, Verdonk ML, Graham B, Saalau-Bethell S, Hamlett CCF, McHardy T, Collins I, Garrett MD, Workman P, Woodhead SJ, Jhoti H, Barford D (2007) A structural comparison of inhibitor binding to PKB, PKA and PKA-PKB chimera. J Mol Biol 367:882–894